1 Stratospheric circulation response to long-lasting Northern high-latitude volcanic eruptions

2

3 Hera Guðlaugsdóttir[1,2], Yannick Peings[2], Davide Zanchettin[3], Gudrun Magnusdottir[2]

4 [1]University of Iceland, institute of Earth Sciences, 102 Reykjavík, Iceland

5 [2]University of California Irvine, Department of Earth System Science, Irvine CA 92697-3100,

6 United States

7 [3]University Ca'Foscari of Venice, department of Environmental Sciences, Informatics and

8 Statistics, 30123 Venice, Italy

9 *Correspondence to:* Hera Guðlaugsdóttir (hera@hi.is)

10

11

12

13

14 Abstract

15 The temporary enhancement of the stratospheric aerosol layer after major explosive volcanic eruptions can

16 trigger climate anomalies beyond the duration of the radiative forcing. Whereas the mechanisms responsible

17 for long-lasting response to volcanic forcing have been extensively investigated for tropical eruptions, less

18 is known about the dynamical response to high-latitude (HL) eruptions. Here we use global climate model

19 simulations of an idealized 6 month long northern hemisphere (NH) high-latitude eruption to investigate

20 the stratospheric circulation response during the first three post-eruption winters. Our results reveal that

21 two competing mechanisms contribute to determining the post-eruption evolution of the NH stratospheric

22 polar vortex: 1) A local stratospheric top-down mechanism whereby increased absorption of thermal

23 radiation by the enhanced aerosol layer yields a polar vortex strengthening via thermal wind response; 2) a

24 bottom-up mechanism whereby anomalous spatio-temporal surface temperature and land-sea thermal

25 contrast yields an increase in atmospheric wave activity that propagates into the winter stratosphere, leading

26 to an increased occurrence of sudden stratospheric warming events (SSWs) and a weakening of the polar

27 vortex. The top-down mechanism dominates over the bottom-up mechanism in winter 1, while the bottom-

28 up mechanism dominates in the follow-up winters. The identification of a deterministic response such as

29 increased SSWs following HL volcanic eruptions calls for increased attention given the widespread surface

30 cooling SSWs can initiate, influence societies throughout the continental NH. Also, the sensitivity of such

31 events to eruption magnitude needs to be evaluated in terms of a possible source of increased seasonal

32 predictability of NH regional climates.

33

1 Introduction

The enhancement of the stratospheric aerosol layer, which typically occurs following strong sulfur-rich explosive volcanic eruptions, is an important driver of natural climate variability by imposing short-lived yet possibly very strong radiative anomalies within the atmospheric column (Robock, 2000; Timmreck, 2012; Zanchettin, 2017). This direct radiative effect can alter both meridional surface and stratospheric temperature gradients that can, in turn, initiate further dynamical climate responses on seasonal to decadal time scales (Church et al., 2005; Gleckler et al., 2006; Stenchikov et al., 2009; Shindell et al., 2009; Otterå et al., 2010; Zanchettin et al., 2012; Swingedouw et al., 2015). Radiative forcing and dynamical responses critically depend on the spatiotemporal characteristics of the enhanced stratospheric aerosol layer, which ultimately depends on the characteristics of the eruption, such as magnitude, timing and location (refs like above).

Spatiotemporal characteristics of volcanic aerosol from high-latitude (HL), Northern Hemisphere (NH) eruptions are typically very different when compared to tropical eruptions. Accordingly, several studies have shown that high-latitude NH eruptions typically initiate different climate responses compared to tropical eruptions (Meronen et al., 2012; Pausata et al., 2015; Guðlaugsdóttir et al., 2018; Zambri et al., 2019; Sjolte et al., 2021). Therefore, tropical eruptions cannot be considered close analogs of high-latitude NH eruptions, underlining the need for more studies on the latter to further quantify their potential climate impacts (Zanchettin et al., 2016).

A major potential distinguishing character between tropical and high latitude NH eruptions concerns the winter stratospheric polar vortex response. When the stratospheric sulfate aerosol layer is enhanced at low latitudes following tropical volcanic eruptions, local warming by infrared absorption increases the meridional stratospheric temperature gradient that can lead to a stratospheric polar vortex strengthening due to a thermal wind response (e.g., Zanchettin et al., 2012, or many others…). Conversely, the local warming from aerosols constrained at higher latitudes decreases the meridional temperature gradient enabling a weakening of the polar vortex (Kodera, 1994; Perlwitz & Graf, 1995; Stenchikov et al., 2002; Oman et al., 2005; Bittner et al., 2016; Sjolte et al., 2021).

A strengthened polar vortex can affect the troposphere as the positive phase of the Northern Annular Mode, while a weaker polar vortex is linked to increased likelihood of sudden

stratospheric warming events (SSWs) in the stratosphere and a negative Northern Annular Mode in the lower troposphere (Haynes, 2005; Domeisen et al., 2020; Huang et al., 2021; Kolstad et al., 2022, and references therein), demonstrating an example of a top-down mechanism.

With its origin in the noisy stratosphere, this top-down mechanism can result in tropospheric signatures following volcanic eruptions. However, the signature tends to be weak in both observations and numerical simulations due to the different realizations and advanced statistical methods needed to extract the signal from the noise (Weierbach et al., 2023; DallaSanta and Polvani, 2023; Kolstad et al., 2022; Azoulay et al., 2021; Polvani et al., 2019; Zanchettin et al., 2022; Toohey et al., 2014). The radiative surface cooling following large volcanic eruptions has been shown to affect the stratospheric polar vortex via a bottom-up mechanism (e.g., Graf et al., 2014; Peings and Magnusdottir, 2015; Omrani et al., 2022). An example of this bottom-up mechanism following HL eruptions is demonstrated in Sjolte et al. (2021) where they linked a weak polar vortex to an increase in wave energy flux from the troposphere to the stratosphere without the meridional stratospheric temperature gradient playing a role.

With this in mind, the importance of transient atmospheric eddies (waves) and eddy-mean flow interferences is becoming increasingly clear in explaining vertical and horizontal mediations of atmospheric perturbations of various origins (e.g., Smith et al., 2022; Nakamura, 2023). DallaSanta et al. (2019) used a hierarchy of simplified atmospheric models to show that eddy feedbacks are crucial in explaining stratospheric-troposphere coupling as well as the stratospheric response alone following a tropical Pinatubo-like eruption. They also identified the extra-tropics as a dominant pathway in which the stratospheric response leads the troposphere following the eruption, a pathway similar to the response to SSWs. This demonstrates that the anomalous atmospheric circulation response following volcanic eruptions does not solely depend on simplified physics via meridional temperature gradients where eddy-mean flow interactions and eddy feedback appear to be essential. Since both mechanisms, i.e., the top-down mechanism triggered by stratospheric heating and the bottom-up mechanism triggered by surface cooling, act together in the real world and, in simulations, under realistic volcanic forcing, idealized model experiments are required to assess their relative contribution to uncertainty in post-eruption regional climate variability (Zanchettin et al., 2016).

Icelandic volcanism has played a role in shaping past NH climate variability and will continue doing so. Two Icelandic eruptions during the past 2000 years, namely Eldgjá in ~939 CE and Laki

3

in 1783 CE, are considered to have had a significant impact on climate variability even on the global scale (Brugnatelli and Tibaldi, 2020; Zambri et al., 2019; Oppenheimer et al., 2018; Thordarson and Self, 2003; Stothers, 1998). These types of effusive eruptions are common in Iceland where their duration can extend over years. During part of the eruption time such eruptions can become explosive (referred to as mixed-phase eruptions) when ascending magma in a conduit comes in contact with water as was considered the case with both Eldgjá and Laki, explaining their widespread impacts. Eruption history as well as dense monitoring network of Icelandic volcanic systems tell us that many of these systems are currently on the verge of an eruption, having already produced some of the largest volcanic eruptions over the past millennia (e.g., Öræfajökull, Bárðabunga and Hekla, Larsen & Guðmundsson, 2014; Barsotti et al., 2018; Einarsson, 2019). Therefore history and current activity makes these types of eruptions an ideal reference case to explore the potential climatic impacts following NH eruptions and to test hypotheses about the underlying mechanisms driving the climate response. This is the focal point of this study where we investigate for the first time the role of wave/eddy activity perturbations and SSWs in the atmospheric circulation response following HL volcanic eruptions. For this we perform idealized, long-lasting HL volcanic perturbation experiments using the Community Earth System Model version 1 (CESM1), both in its coupled and atmosphere-standalone modes. We begin our investigation in the NH stratosphere followed by troposphere to evaluate the response during the first three winters following the eruption, referred to as post-eruption winters in the text, and assess the dominating mechanism in each winter. This paper is organized as follows: Section 2 describes the model, experimental design and diagnostics, results are presented in section 3 and we end with summarizing discussions in section 4.

2 Methods

2.1. Numerical Model

We use the Community Earth System Model (CESM) version 1, developed by the National Center for Atmospheric Research (NCAR). In our configuration of CESM1, the atmospheric component is the Whole Atmosphere Community Climate Model, version 4 (WACCM4, Marsh et al, 2013). WACCM4 includes 66 vertical levels (up to 5.1×10^{-6} hPa, ~140 km) and uses CAM4 physics. We use the specified chemistry version of WACCM4 (SC-WACCM4), which is computationally less expensive to run, but simulates dynamical stratosphere-troposphere coupling and stratospheric

variability like SSWs and the polar vortex with skills comparable to the interactive chemistry model version (Smith et al., 2014). CESM1/WACCM4 uses the Community Atmospheric Model Radiative Transfer (CAMRT) to parameterize the radiative forcing where it has been shown to accurately represent stratospheric aerosols by f. ex. simulating the temperature response following Mt. Pinatubo in 1991 (Neely et al., 2016). The SC-WACCM4 experiments are run with a horizontal resolution of 1.9° latitude by 2.5° longitude and include present-day (year 2000) radiative forcing. A repeating 28-month full cycle of the Quasi-biennial Oscillation (QBO) is included in the SC-WACCM4 experiments through nudging of the equatorial stratospheric winds to observed radiosonde data. In the coupled ocean-atmosphere configuration, the ocean component of CESM1 is the Parallel Ocean Program version 2 (POP2). CESM1 also includes the Los Alamos sea-ice model (CICE), the Community Land Model version 4 (CLM4) and the River Transport Model (RTM). CLM is run at a horizontal resolution of 1.9°x2.5°, POP2 and CICE are run at nominal 1° resolution with higher resolution near the equator than at the poles. Further details about CESM1 are given in Hurrell et al. (2013).

2.2. Volcanic Forcing File

We use the Easy Volcanic Aerosol (EVA) forcing generator (Toohey et al., 2016). EVA provides zonally symmetric stratospheric aerosol optical properties as a function of time, latitude, height, and wavelength (see detailed information on the tool in Toohey et al., 2016). EVA has been used to generate volcanic forcing in both idealized volcanic experiments (e.g., Zanchettin et al., 2016) and realistic paleoclimate simulations (Jungclaus et al., 2017) contributing to the sixth phase of the coupled model intercomparison project.

We use EVA to prescribe the volcanic aerosol loading corresponding to that of the 1991 Mt. Pinatubo eruption (14.04 Tg SO_2), but at 45° N. Since the model reads the volcanic forcing as aerosol mass (kg/kg), we scale our forcing file by using the standard aerosol mass input file for CAM4 and 5 (see Neely et al., 2016, Table 1) for the same eruption. A monthly scaling factor was derived from this linear relationship between the aerosol extinction ($1/m^2$) and the aerosol mass (kg/kg) that was used to scale the raw EVA forcing data (Fig. 1). From these scaled forcing data, the aerosol optical properties for our experiments are obtained with a two-step approach. First, we move the injection location northwards so that the center of the aerosol mass is at 65° N latitude and spans 10-28 km in altitude. Then, we define the start of the eruption to be May 1st and prolong

402 the peak of the forcing by extending in time the highest monthly value in the so-obtained forcing

403 data, so that the decline in aerosol mass begins 6 months after the start of the eruption or on October

404 1 (see Fig. 1). We thus obtain aerosol optical properties for an idealized, long-lasting high-latitude

405 NH eruption. In this experiment we assume stratospheric injection only, although similar eruptions

406 in the natural world would likely inject part of the total aerosol mass within the troposphere during

407 the eruption. Past NH eruptions like Laki and Eldgjá had an atmospheric loading of 210Tg and

408 120Tg respectively, much larger than our 14Tg eruption, that was carried aloft with the eruptive

409 column up into the upper troposphere with portions of the aerosols reaching the lower stratosphere

410 during the eruptions (Thordarson et al., 2001). Hence our experiment can also be considered as a

411 6-month stratospheric aerosol injection that is analogous to similar although smaller eruptions (as

412 compared to Laki) without the tropospheric aerosols.

413

414
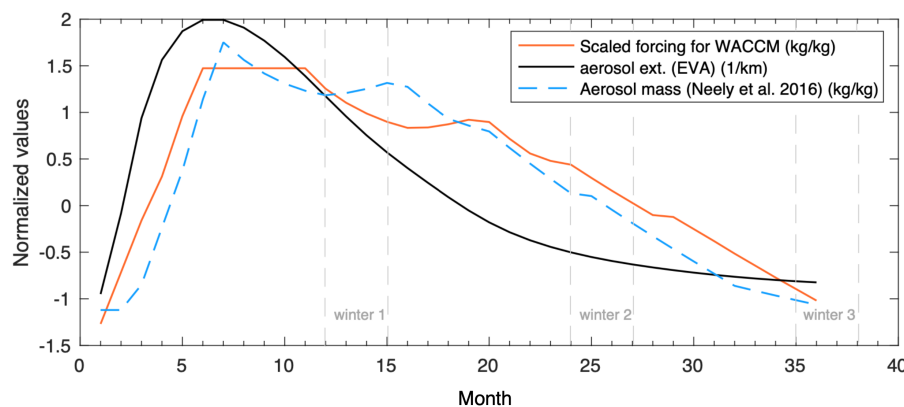
415 Figure 1: The time series of the original EVA aerosol extinction output (1/km, black curve) and the

416 aerosol mass of the volcanic forcing file of Neely et al. (2016) (kg/kg, blue dashed curve) used for

417 deriving the linear scaling coefficient for the conversion of EVA output into WACCM4 input

418 (kg/kg, red curve). The time series are normalized (mean=0, standard deviation=1) to allow

419 comparison of time series with different units. The horizontal axis is time (months) from the start

420 of the eruption. Here we assume that the aerosol lifetime at 65° N is the same as at 45° N. Dashed

421 vertical lines show the three winters that we focus on in this study.

422

423

2.3. Experimental design

We ran two volcanic perturbation experiments with CESM1. The first experiment is conducted with the atmosphere-only version of the model, where boundaries to SC-WACCM4 are provided by prescribed fields of sea-surface temperature (SST) and sea-ice concentration (SIC) corresponding to the 1979-2008 monthly climatology of HadISST observations (Rayner et al., 2003). We refer to this experiment as *atm-only*. The second experiment is conducted with the coupled version of the model, henceforth referred to as *cpl*. For each experiment we run 20 ensemble members including the volcanic forcing and 20 paired ensemble members without the volcanic forcing and otherwise identical to the volcanic simulations, which we refer to as the control.

The atmosphere-only experiments were run over three full years, which provides two full winters after the onset of the eruption. We found that there was no need to extend the simulations further given the duration of the forcing and short memory of the atmosphere. The coupled experiments follow a similar protocol but they were integrated over 15 years to assess the response influenced by oceanic dynamical adjustment. However, in this study we only focus on the first three winters following the eruption. We define the first post-volcanic winter as December of the starting year (year 0) and the following January and February (year 1), the second post-volcanic winter is then December of year 1 and the following January and February of year 2 etc.

Because the QBO is prescribed, and given its importance for the atmospheric circulation and the distribution of volcanic aerosols within the stratosphere (Thomas et al., 2009; DallaSanta et al., 2021; Brown et al., 2023), we have been careful to homogeneously sampling the QBO phasing that is imposed on the 20 ensemble members. For this, we shift the 28-month QBO cycle by one month for every ensemble member, so that the phasing of the QBO differs from one ensemble member to the next (Elsbury et al., 2021). This avoids potential biases in the climatic response that may be induced by any dominating QBO phase.

2.4. Diagnostics

Model output is analyzed by computing paired anomalies, defined as deviations of each volcanic simulation from the corresponding control simulation (Zanchettin et al., 2022) (volcanic minus control). The statistical significance of the ensemble mean of paired anomalies is assessed at the

514 95% confidence interval, calculated from all 20 ensemble members, using a two-sided student's t-
515 test in addition to a Kolmogorov-Smirnov test.
516 To evaluate the effects of planetary waves on the zonally-averaged stratospheric response, we use
517 the Eliassen Palm (EP) flux, and its divergence (Edmon et al., 1980) in addition to the 3D
518 generalization of the EP flux, the Plumb flux (Plumb, 1985), for a longitudinal representation in
519 the lower troposphere and stratosphere. We identify SSW events by using an algorithm following
520 the procedures described in Charlton and Polvani (2007), where mid-winter sudden warming
521 events are determined to take place if the 10 hPa zonal-mean zonal wind at 60°N becomes easterly.
522 Once a warming is identified, no day within 20 days of a central date, defined as the first day in
523 which the daily mean zonal mean wind at 60N and 10hPa is easterly, can be defined as an SSW.
524 For the eddy feedback calculations we compute the square of the local correlation across the
525 ensemble members between DJF zonal mean zonal wind and the divergence of the northward EP
526 flux (delta phi F phi) averaged over 600-200 hPa (Smith et al. 2022). In addition, we compute the
527 rate of temperature changes in the 2m temperature (T2m) gradient using spherical harmonics to
528 yield a T2m gradient in the meridional (dZ/dlat) and zonal (dZ/dlon) directions.
529
530 **3 Results**
531 In the following sections we will investigate the cpl experiment to characterize the forced response
532 and identify the mechanism by utilizing the information provided by the *atm-only* experiment. We
533 begin our investigation in the upper atmosphere before making our way towards the surface.
534
535 **3.1. Volcanic radiative forcing**
536 The net shortwave (SW) and longwave (LW) downward flux at the top of the atmosphere show an
537 expected behavior following a stratospheric sulfate injection where we see a decrease in the SW
538 due to scattering and a decrease in the LW due to absorption around the injection location (Fig. 2c-
539 f). The perturbation of SW fluxes for both *cpl* and *atm-only* is influenced by the obvious strong
540 seasonal evolution in solar insolation, where we see strong anomalies during the first summer north
541 of 30° N than then becomes more confined to the mid latitudes as winter progresses with a slow
542 decrease towards the end of the third year (Fig. 2c-d).
543 LW anomalies also show seasonal evolution with stronger LW flux at mid latitudes compared to
544 at high latitudes during summer that continues into the winter season and remains significant

throughout most of these three years. During winter, the LW anomalies are present at high latitudes where the SW anomalies are absent. The latitudinal bands of radiative flux anomalies correspond to the maximum values of the aerosol mass between 60 and 70° N, and the aerosol mass being largely confined north of 45° N (Fig. 2a-b). Overall, the radiative forcing thus remains largely confined to NH extratropical summers with the exception of a slight significant increase around 30-60° S in the second and third summer (Fig. 2c-d) that is visible at around 14-15 km a.s. (Fig. 2b). This occurs due to spatial features in the Neely et al. (2016) aerosol forcing that we use for scaling, where a slight aerosol increase occurs at lower latitudes, although this is not detectable when the aerosol mass is averaged through the atmospheric column with respect to time (Fig. 2a).
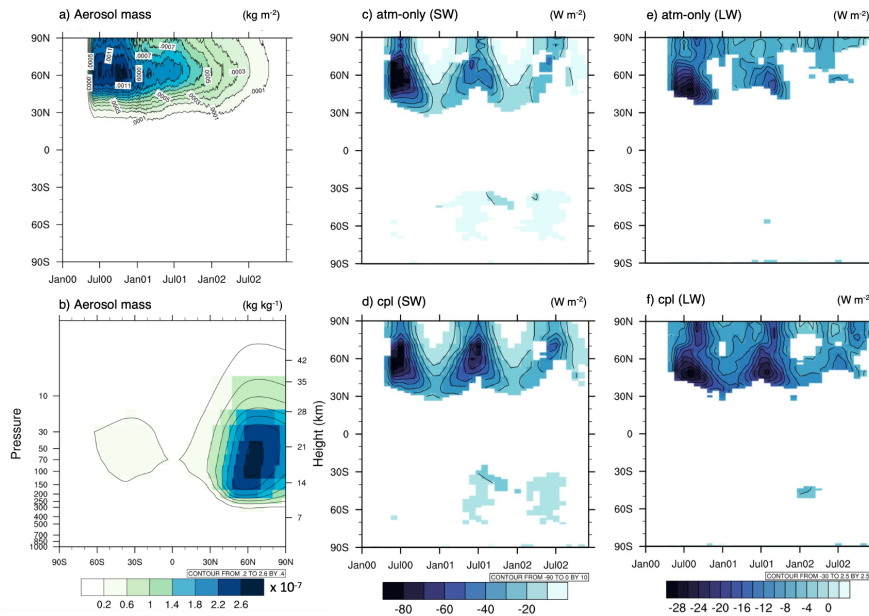
Figure 2: Left panels: a) Average aerosol column mass time evolution in kg/m2 and b) pressure vs. latitude slice of the aerosol mass in kg/kg (3-year average). Aerosol mass is the same in cpl and atm-only. c) and d) show the time evolution of the net SW flux (downward) anomaly at the top of the atmosphere, and e) and f) the same but for net LW flux anomaly, resulting from the volcanic

646 aerosol mass, in c) *atm-only* and d) *cpl* where coloured areas indicate 99% significance compared
647 to the control experiment.
648
649 **3.2. Stratospheric response**
650 The strong seasonality in the LW perturbations described above also characterizes stratospheric
651 temperatures, where a strong increase in the zonally averaged temperature at 50 hPa (T50) is
652 detected north of 30° N during post-eruption summers in both experiments (Fig. 3a and 3b). This
653 summer warming is followed by a net cooling of the polar stratosphere in the first winter seen for
654 both *cpl* and *atm-only*. A clear difference in the T50 response in the two experiments is seen in
655 winter 2, where *cpl* yields warming over polar latitudes while *atm-only* yields cooling (Fig. 3a,b),
656 revealing the intra-seasonal dynamical effects in the *cpl* experiment beyond the direct radiative
657 response as we will see later on. The contrasting temperature response is accompanied by an
658 opposite response in the zonal-mean zonal winds at 10hPa (U10) between 70 and 80° N, indicating
659 the state of the polar vortex, where a polar vortex weakening is detected in winter 2 for *cpl* but a
660 strengthening *atm-only* (Fig. 3c-d). Figures 3c-d do show a large ensemble spread in the zonal
661 mean U10 winter response that is evident of a low signal to noise ratio. While the first winter in
662 *cpl* and the first two in *atm-only* show little statistical significance, according to a Kolmogorov-
663 Smirnov test, this significance does increases for winter 2 in the *cpl* experiment. We also see this
664 weakening in the zonal mean U50, also showing stronger significance during winter,
665 (Supplementary Fig. S3) but not as clearly as in the zonal mean U10. However, for consistency we
666 will mainly be focusing on the U50 response in the following section where this response is clear
667 over the NH polar cap. The difference between *cpl* and *atm-only* will be in the focus in the
668 following sections.
669

Deleted:

a) T50 (cpl)

CONTOUR FROM -12 TO 12 BY 2

-12 -8 -4 0 4 8 12 °C

685

b) T50 (atm-only)

CONTOUR FROM -10 TO 12 BY 2

-10 -6 -2 2 6 10 °C

686

11

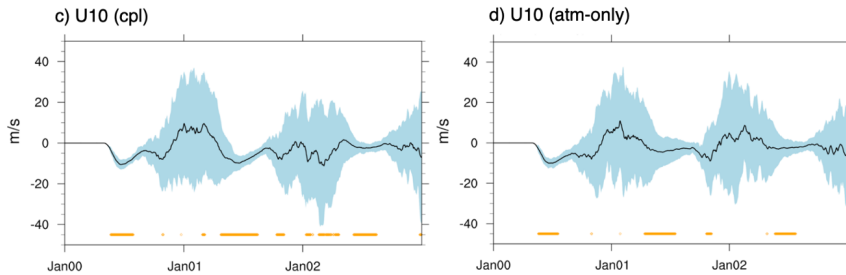c) U10 (cpl)

d) U10 (atm-only)

689
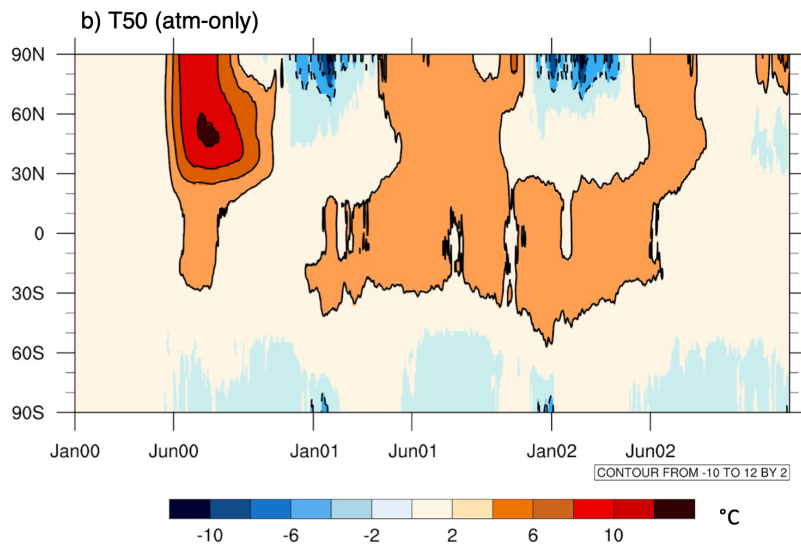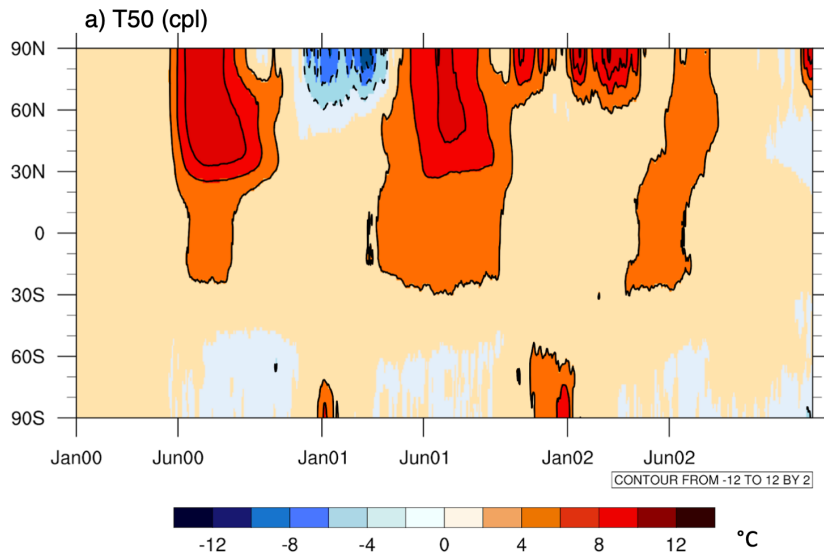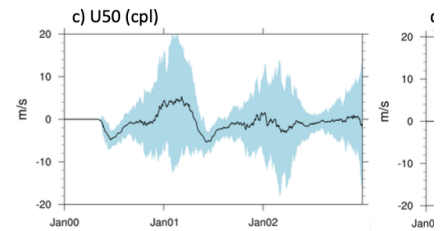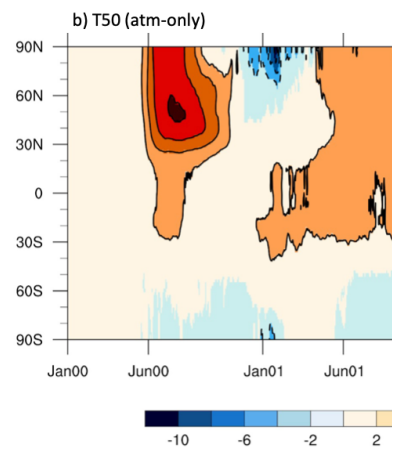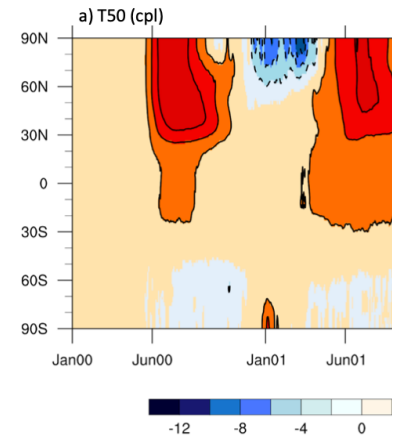
690 Figure 3. a,b) Latitude versus time response of T50 anomalies in a) *cpl* and b) *atm-only*. Contours

691 are significant in 95% confidence intervals according to a student's t-test. c,d) Stratospheric polar

692 vortex response shown as the zonal mean U10 anomalies between 70 and 80° N for c) *cpl* and d)

693 *atm-only.* Black lines show the ensemble mean anomalies and blue shadings show the ensemble

694 +/- 2 standard deviation anomaly range. Orange markers indicate when the difference between

695 perturbed and unperturbed experiments becomes significant (p<0.05) according to a Kolmogorov-

696 Smirnov test.

697

698 **3.2.1 - First post-eruption winter**

699 In the cpl experiment, the polar vortex strengthening in winter 1 is associated with extensive

700 anomalies in temperature and zonal wind at 50 hPa (Fig. 4a). The anomalous temperature pattern

701 consists of cooling at high latitudes and into the midlatitudes over the Atlantic, and warming over

702 large swaths of the subtropics (to 20° N) and into the midlatitudes over the Pacific, also identified

703 in the zonal mean T50 (Fig. 3b). Similarly, the zonal wind weakens into the midlatitudes over the

704 Pacific while it is stronger in mid to high latitudes over the Atlantic. The strong upward EP flux

705 (black arrows) is an indicator of the direction of propagated waves originating at the surface around

706 the midlatitudes, where the horizontal and vertical EP flux components can be considered

707 proportional to both eddy heat and momentum flux (Fig. 4d). A convergence (negative divergence,

708 dashed red contours) in the wave flux is detected in the upper troposphere that acts towards

709 weakening the tropospheric westerlies (Fig. 4d and Supplementary Fig. S2) while the EP flux and

710 its convergence within the stratosphere does not appear to impact the stratospheric mean flow and

711 the polar vortex. Therefore, the local heating due to the volcanic aerosols and the associated

712 increase in the meridional temperature gradient in the stratosphere appear to dominate the eruption

713 dynamics of the polar vortex via thermal wind response, also depicted by the LW anomalies (Fig.

12

787 2f). Winter 1 in *atm-only* shows a similar thermal wind mechanism at play in the stratosphere as

788 for the *cpl* experiment (Fig. 5a and 4a, respectively), in this case with the obvious less tropospheric

789 influences - due to lack of forced surface cooling - as seen in the limited anomalous upward wave

790 activity detected by the EP flux diagnostics (Fig. 5c).

791

792
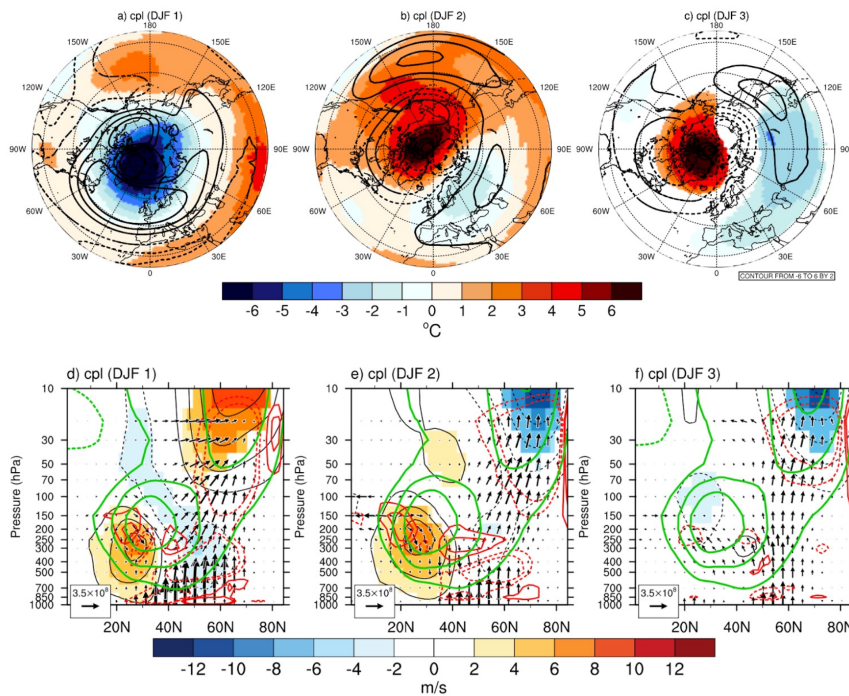
793 Figure 4: Winter stratospheric response in the *cpl* experiment. a-c) U50 (contours) and T50

794 (shading: red = warming, blue = cooling) response for winters 1-3, respectively. d-f) EP flux

795 (arrows) and divergence (red contours) response, along with zonal-mean zonal wind response

796 (black contours and shading: red = strengthening, blue = weakening) and climatology (green

797 contours) in winters 1-3, respectively. Contours and color-shaded areas indicate 95% significance

798 according to a student's t-test. Only vectors that are significant at the 95% confidence interval are
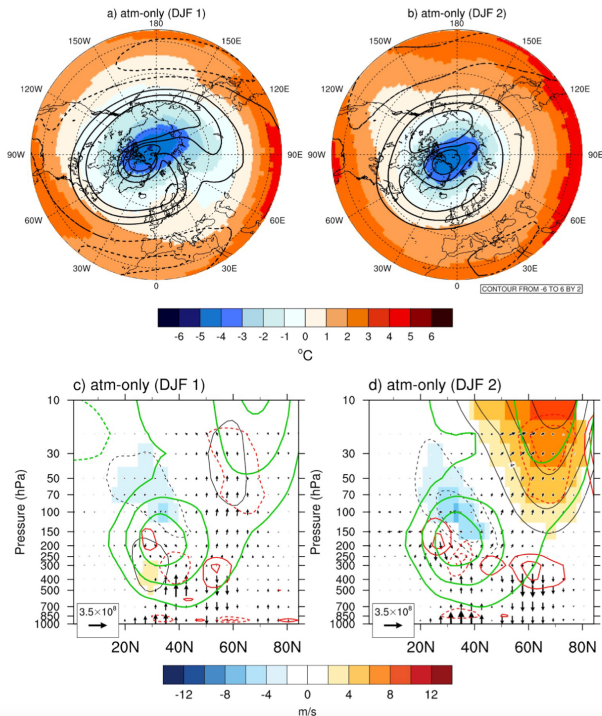
799 shown.

800

13

Figure 5: The same as Fig. 4 but for the *atm-only* experiment. a-b) Zonal wind (contours) and temperature (shading) response at 50 hPa for winter 1 and winter 2, respectively. c-d) EP flux (arrows) and divergence (red contours) response along with zonal-mean zonal wind (black contours) and climatology (green contours, 2m) in winters 1-2, respectively. Contours and colored area indicate 95% significance according to a student's t-test.

3.2.2. Second post-eruption winter

A stark difference in the polar vortex response is detected between *cpl* and *atm-only* in winter 2. While *atm-only* exhibits a response similar to winter 1 (Fig. 5b), a significant warming over North America and the North Pacific emerges in *cpl* along with a weakening of U50 at high latitudes (Fig. 4b) indicating a shift of the polar vortex towards Eurasia. This warming at high latitudes then coincides with a slight LW absorption at high latitudes (Fig. 2f). The U50 weakening is not uniform throughout the longitudes explaining the lack of response detected in the zonal mean U50

(Supplementary Fig. S3), where one needs to go above 50hPa, to U10, to get a clear response in the zonal mean zonal wind (Fig. 3c). An anomalously strong upward propagation of planetary waves persists in the *cpl* (Fig. 4e), with a stronger upward EP flux now protruding into the stratosphere above 20hPa in contrast to winter 1. The upward EP flux and its convergence in the polar stratosphere are evident of their contribution towards the weakening of the U50 and a general dominance over the effects of thermal forcing by aerosols that have been, at this stage, substantially reduced (Fig. 1).

Similar wave reflection pattern as identified in the *cpl* experiment is known to be associated with SSWs, where we suspect that the decrease in the T50 difference between mid latitudes and the pole can act as a trigger for a weaker polar vortex in addition to the stratosphere absorbing the upward propagating waves that is known to cause warming over the polar cap (Kodera et al., 2016; Kretschmer et al., 2018). We will see further evidence of this in the next section.

3.2.3. Third post-eruption winter

The results in this section only refer to the *cpl* experiment since winter 3 is lacking in *atm-only*. The SSW-like pattern of winter 2 clearly continues into winter 3, where most of the volcanic aerosols have decreased to the extent that their radiative impacts no longer dominate, except that the T50 warming is now confined over the polar stratosphere (Fig. 4c). Anomalous upward propagation of planetary waves continues to persist (Fig. 4f). This upward wave flux in addition to the T50 warming resembles a pattern that behaves much like absorbing SSWs defined by Kodera et al. (2016). To examine this response further we define SSWs based on the reversal of the zonal mean zonal winds at 60° N and at 10hPa between November and March according to the method of Charlton and Polvani (2007).

Results from the SSW analysis are presented in Fig. 6. No significant increase in SSWs is found in winter 2, despite the SSW-like pattern detected. This changes in winter 3 when the difference between perturbed and unperturbed experiment becomes statistically significant, with 27 SSWs occurring in our forced experiment compared to only 6 in the control experiment (p-value = 2.6e-4). This increase in SSWs agrees well with the U50 and T50 anomalies of winter 3 (Fig. 4c). During winter 2, the warming of the polar stratosphere is as strong as in winter 3 but more spread out into midlatitudes. Although the response in winter 2 does not lead to as many SSWs despite

the weaker zonal winds, it does appear to act as an important precursor to the significant increase in SSWs detected in winter 3. These results are also in agreement with the stratospheric Plumb flux in winter 3 (Supplementary Fig. S1c) where the upward flux is mostly circumpolar between 40° and 60° N and evident of SSWs.
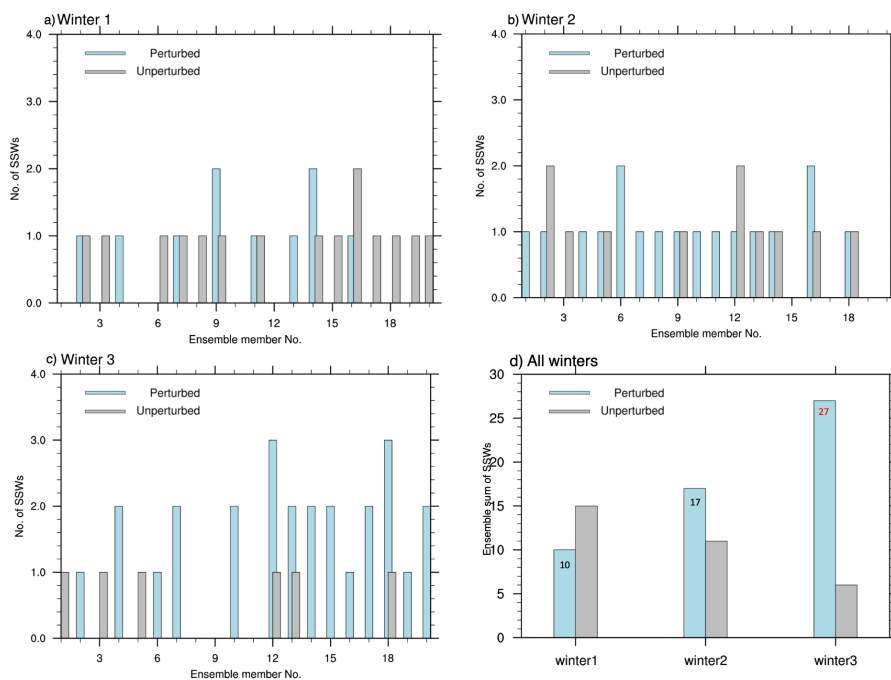

Figure 6: a-c) The number of SSWs during winters 1-3 for each ensemble member in the *cpl* experiment and d) The sum of all SSWs in each experiment for all 20 ensemble members of winters 1-3 both for *cpl* (light-blue bars) and control (gray bars). The color red indicates 95% significance according to a two-sided student's t test.

When comparing the ensemble sum of SSWs in the perturbed and unperturbed experiment using a Kolmogorov-Smirnov test (Fig. 5d), a significant increase in the number of SSWs occurs in winter 3 (p=0.0135). This underlines the generally strong SSW response occurring in winter 3, when the fraction of ensemble members having more than 1 SSW per winter increases to 50% (10

ensemble members) in winter 3 compared to only 10% in winters 1-2. Of these 10 ensemble members, two members show three SSWs per winter that can be considered highly unlikely based on historical records: Despite winters with more than 1 SSWs are considered unusual, examples do exist in the observational record of multiple SSWs in one winter, like the winter of 1998/1999 and 2009/2010 (Kodera et al., 2016 and Ineson et al., 2023 respectively). However, when considering the different number of SSWs between winters in the unperturbed experiment we cannot rule out the possibility that large ensembles are needed to confirm this link.

According to the above, the evolution in *cpl* from winter 1 to winter 3 can be summarized as follows: In the first winter, the thermal forcing appears to be stronger than the upward wave flux because of the large amount of aerosols present, thereby dominating the response that causes the polar vortex strengthening and the inclusion of cold polar air within. In the second winter, the thermal forcing from the volcanic aerosols at midlatitudes has decreased where it is now mostly confined to higher latitudes as seen both in the LW flux and T50 (Fig. 2f and Fig. 3b). We suspect that in addition to the aerosol decrease, this slight decrease in the temperature difference between high and midlatitudes allows the strong upward wave flux to dominate and enter the upper stratosphere. There the waves are absorbed that causes further warming over the polar cap in addition to weakening the zonal stratospheric winds (Fig. 5b and Fig. 4b). This upward wave flux and weaker winds continue into the third winter, where winter 2 likely acts as a precursor, allowing for SSWs to develop more frequently as detected in the T50 warming that is now confined over the polar cap (Fig. 4c and Fig. 5c, respectively). The expected absence of a surface response is obvious in our *atm-only* experiment where basic physical mechanism, via the thermal wind balance due to radiative heating, dominates the atmospheric circulation response in the first two post-eruptive winters, with a strong stratospheric polar vortex isolating the cold air over the polar regions in the second winter as in the *cpl* experiment (Fig. 5a-b).

3.3. Tropospheric response

What is it then that drives this polar vortex weakening and the SSW response in the *cpl* experiment? To understand better, we now turn our attention towards the troposphere to evaluate the role of eddies and surface cooling in the forced *cpl* response.

3.3.1. The role of eddy feedback

As detailed in the introduction, the mechanism behind a stratospheric polar vortex response following large volcanic eruptions has long been considered to be rooted in anomalous changes within the stratospheric temperature gradient, whereas in recent years number of studies have been emerging with evidences depicting tropospheric eddies as the main force in mediating atmospheric circulation responses towards the stratosphere and vice versa. We want to examine further if eddies play a role in the *cpl* polar vortex response and the upward EP flux detected (Fig. 4a-f) as well as the SSW detected in the 3rd winter, where we follow Smith et al. (2022) to calculate the eddy feedback as the squared of the correlation between the zonal mean zonal winds (U) and the divergence of the EP flux averaged over 200-600hPa. This is done for both perturbed (red) and unperturbed (blue) experiments (Fig.6).
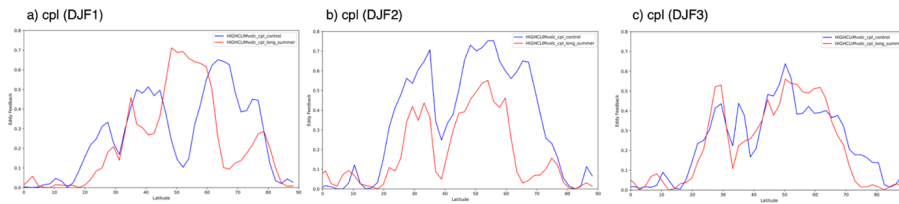

Figure 6: The *cpl* eddy feedback evolution in the lower atmosphere (200-600hPa) in winters 1-3 where the eddy feedback is calculated as the squared correlation of zonal mean zonal winds and the divergence.

An increase in perturbed eddy feedback at 45-60° N in winter 1 occurs during the strong thermal forcing and the polar vortex strengthening and implies eddy mean-flow interactions and increased eddy generation (Fig. 6a). Interestingly, a similar trend is also detected in *atm-only* for both winters (Supplementary Fig. S4) where the aerosol thermal forcing dominates within the stratosphere. This is especially clear in winter 2 of atm-only where a more robust increase in eddy feedback occurs at 35-70° N. Since the thermal wind balance is strongest during boreal summer, as seen in the increase in LW flux at mid-latitudes for both *cpl* and *atm-only,* but close to normal during winter in *atm-only,* where LW flux is absent at mid-latitudes, it suggests that although thermal forcing triggers the polar vortex strengthening the eddy feedback maintains it. However, we cannot

18

exclude the possibility that the DJF polar vortex strengthening mainly depends on the thermal wind balance during summer that continues into early winter (e.g. July-November) without eddies playing a role. DallaSanta et al. (2019) reported on the role of eddy feedback in the polar vortex strengthening following a Pinatubo-like volcanic eruption. One of their conclusions were that the thermal-wind balance is too simplified in explaining the simulated stratospheric polar vortex response where eddies are needed to mediate atmospheric perturbation, both to couple the stratosphere to the troposphere as well as achieving the forced stratospheric response alone. Although our eddy feedback results suggest a similar response as in DallaSanta et al. the signal appears to be quite low compared to the noise as is depicted by the variability between winters in the unperturbed experiment.

The role of eddies in the polar vortex weakening in winters 2-3 is even less clear, especially considering the eddy feedback increase of the control run in winter 2 suggesting in general that more ensemble members are needed to evaluate the role of eddies in the forced response with any certainty. However, we do see evidence of eddy-mean flow interactions of opposite signs in winter 2, suggesting that reduction of eddy feedback (eddy growth) is occurring due to wave breaking in the upper stratosphere at high latitudes as is identified in the EP-flux and the weakening the zonal winds (Fig. 6b and Fig. 4e respectively). Finally, the feedback pattern emerging in the third winter does not seem to be related to the upward wave activity (Fig. 4f) and thus possibly demonstrating a top-down mechanism via the extratropics, a pathway that is known to be similar to the response to SSWs (DallaSanta et al., 2019). In addition to the relatively low signal to noise identified in the eddy feedback, it is also important to consider that Smith et al. (2022) identified CESM1 WACCM-SC as having one of the weakest eddy feedback of the sixteen models they investigated. Nonetheless they do underline the need for further studies on this subject.

To examine in more detail the origin of the upward wave fluxes in winters 2 and 3 of the cpl experiment that causes the detected polar vortex weakening and the SSWs, we look towards the surface.

3.3.2. The role of surface cooling

As a response to the decrease in SW flux following the eruption, extensive and heterogeneous cooling is identified in the T2m anomalies in winters 1-3 over latitude bands that contain the most significant SW flux decrease (Fig. 2d and Fig. 7). At hemispheric scale we see the strongest cooling

19

over northeastern North America and along the Asian midlatitudes in winter 1 that protrudes over the northwestern North Pacific (Fig. 7a) where it progresses from an initial preferential surface cooling over the midlatitudes in winter 1 to a later cooling of polar regions in winter 3.
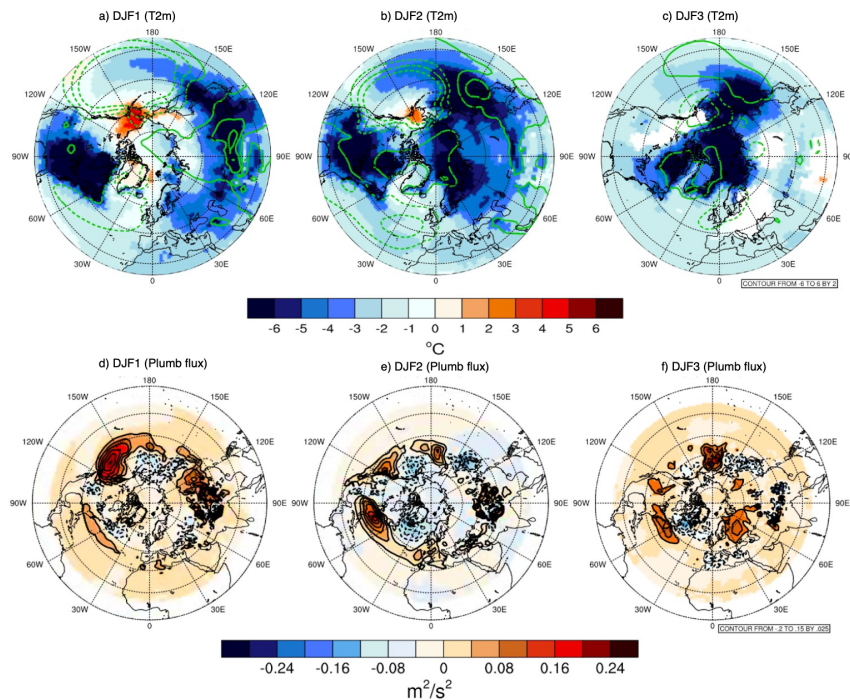

Figure 7: a-c) Sea level pressure (contours) and temperature (T2m, colored area) anomalies in *cpl*, for winter 1-3, respectively. d-f) Vertical component of the Plumb flux response at 850 hPa for winters 1-3, respectively. Contours and shaded areas indicate significance at the 95% confidence interval according to a student's t-test.

a) DJF1 (T2m) b) DJF2 (T2m)

c) DJF1 (Plumb flux) d) DJF2 (Plumb flux)

Figure 8: Same as Figure 7 but for winters 1-2 in *atm-only*.

This T2m cooling in winter 3 (Fig. 7c) occurs during the significant increase in SSWs also detected in winter 3 (Fig. 5), an expected cooling pattern during such events. In general the large-scale circulation is rather consistent in winters 1 and 2, where it is largely constrained by the imposed SSTs and hence land-sea contrast dynamics. In *atm-only*, the surface response is hampered over the ocean by construction, and T2m anomalies are therefore confined to landmasses, yielding an overall much weaker temperature response compared to *cpl* (Fig. 8a-b).

Apart from the magnitude of the cooling, the main difference between the surface temperature responses in *cpl* and *atm-only* is the presence of anomalous warming-cooling dipoles, hence regions of enhanced temperature contrast like the Aleutian/Alaska region. The vertical component of the 3D wave activity flux (the Plumb flux) at 850 hPa (Fig. 7d-f) allows us to locate the origins of the upward *cpl* EP flux (Fig. 4d-f) as being strongest over the north eastern part of the Pacific

Ocean (off the west coast of North America) in winter 1, where it continues up into the stratosphere at 150 hPa (see Supplementary Fig. S1a). In winter 2, the vertical Plumb flux has decreases in the North Pacific and increases over the North Atlantic and Siberia, pointing to a possible influence of the change in land-sea temperature contrast (Fig. 7e). In addition to this upward flux, we also detect downward propagating wave flux over both the Aleutian and Greenland regions at 850 hPa and over a large area south of 45° N at 150 hPa. This downward Plumb flux is evidence of changes in the planetary wave structure where wave reflection occurs due to the sudden weakening of the zonal winds identified in the U10 (Fig. 3a).

An upward wave-activity flux now dominating both at 850 (seen in Fig. 7f) and 150 hPa (Fig. S1c), where it encircles the polar stratosphere north of 60° N.

Only minor activity is occurring in the Plumb flux of *atm-only* in winter 1 as expected, where downward flux dominates the mid-latitudes, with the exception of the upward flux over Greenland and the Himalayas that is most likely of orographic nature (Fig. 8c-d).

When the cooling is no longer confined to the NH mid-latitudes in *cpl* and has reduced towards the polar regions as in winter 3, also evident in the SST (Supplementary Fig. 5S), the upward Plumb flux also decreases compared to previous winters (Fig. 7f). This suggests that the mid-latitude spatiotemporal cooling pattern plays a part in the strong wave activity detected. This can be revealed by computing the T2m gradient (Tgrad) where strong land-sea temperature gradients are known for their ability to influence atmospheric wave activity (Hoskins and Valdes, 1990; Brayshaw et al., 2009; He et al., 2014; Wake et al., 2014; Portal et al., 2022). In winter 1 the meridional gradient shows sharp significant changes encircling 45° N (Fig. 9a), with positive (negative) gradient anomalies occurring south (north) of 45° N. In winter 2 we still see the gradient present at 45° N but now located over North America and the North Pacific while winter 3 mostly reveals regional anomalies in the Barents-Kara, Greenland-Iceland and the North Pacific regions (Figure 9b-c), occurring over areas of significant sea ice increase (not shown). The sharp Tgrad changes throughout the NH at 45° N identified in winter 1 (Fig. 9a), followed by a reduction of land-sea temperature contrast over eastern Canada and the U.S. in winter 2 (Fig. 7b), a known cause of planetary wave enhancement (Portal et al., 2022), could provide an explanation for the strong upward wave flux detected in the second and third post-volcanic winters (Figure 7e-f). Both the zonal and meridional Tgrad components show an increase in the northern part of Alaska that

Deleted: 8d

Deleted: cooling is confined to the midlatitudes only, while the warming is located

Formatted: Font colour: Auto, Ligatures: Standard + Contextual

Formatted: Font colour: Auto, Ligatures: Standard + Contextual

Deleted: (Fig. 8e).

Formatted: Font colour: Auto, Ligatures: Standard + Contextual

Formatted: Font colour: Auto, Ligatures: Standard + Contextual

Deleted: ¶
4 Summarizing discussions

22

coincides with the region of T2m warming over the Aleutian/Alaska region (Fig. 7a) and the strong upward Plumb flux (Fig. 7d). This warming, in addition to the strong continental cooling over North East America and the general decrease in Tgrad spanning from mid to northern part of North America, might also trigger this strong Plumb flux in the Northern Pacific. At least it is unlikely that the Tgrad alone could explain such a strong increase in the upward Plumb flux where the source is likely to be rooted in anomalous spatial temperature patterns. Although not shown, an increase in sea ice extent in East Siberia extending into the Chukchi Sea, in addition to the temperature dipole over Alaska and North East America, might further support the role of anomalous spatial temperature pattern occurring in the vicinity of this strong upward Plumb flux detected.

Plotting the average Tgrad for various regions against the average number of SSWs for winters 1-3 (Supplementaru Fig. S6), we do see that the strongest Tgrad reduction occurs over the North East US in the second winter, agreeing with the upward Plumb flux over the same region and serving as further evidence for its contribution to the upward EP flux in winter 2. This Tgrad reduction continues into the third winter where we also detected a reduction in the upward Plumb flux over the same area (Fig. 7f). Looking towards the Barents sea, a clear spatial difference emerges compared to the North East US, where a clear Tgrad increase occurs in winter 3 related to the SSWs. In general less changes are detected between winters in the North West NA and the North Pacific, reflecting the confined cooling over higher latitudes in winter 3 associated with the SSWs.

23
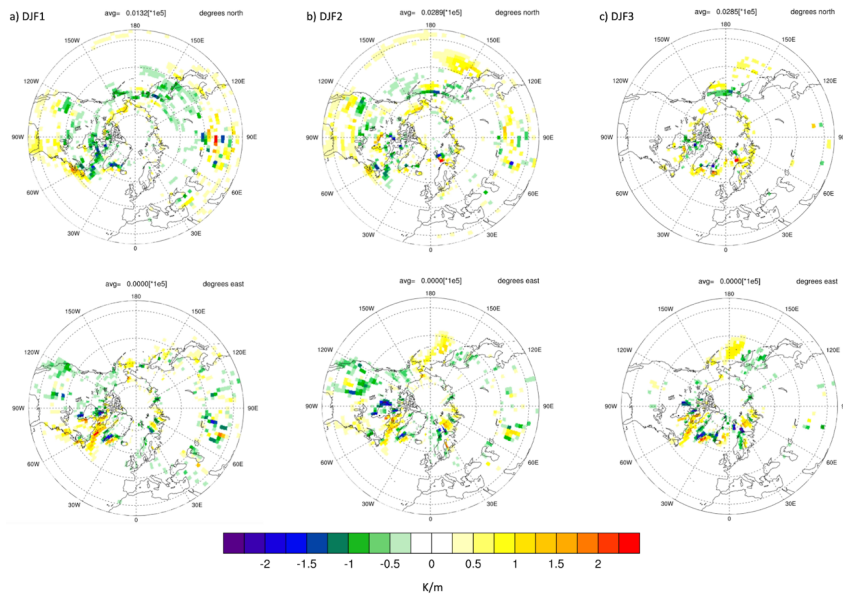
Figure 9: a-c) The zonal (degrees north) and meridional (degrees east) T2m gradient anomalies (perturbed minus unperturbed) for winters 1-3. Colored areas indicate 95% significance according to a student's t-test.

4 Discussions

Our two sets of coupled ocean-atmosphere and atmosphere-only experiments examine the large-scale climate response to an idealized long-lasting NH eruption, where their differences give us valuable insight into the volcanically forced mechanisms at play within the coupled climate system in CESM1. We assessed the first three winters of the *cpl* experiment and used the first two winters of *atm-only* as a comparison to investigate the dynamics that govern the stratospheric polar vortex and the associated surface response.

Results from our *cpl* experiment show a similar response in the first winter as in the two winters of *atm-only*, with a strengthening of the zonal winds resulting from an aerosol-induced sharp temperature gradient between the mid-latitudes and the pole (Fig. 4a and Fig. 5a). We show that this zonal wind strengthening is not affected by the strong upward EP flux detected, where the LW flux (Fig. e-f) supports our conclusions that the polar vortex strengthening is induced by the

24

1832 thermal wind balance. A distinct change to this pattern emerges in *cpl* winter 2 where we detect an

1833 SSW-like pattern, with strong negative anomalies emerging in the polar U50 winds and a warming

1834 in the T50 field (Fig. 4b). We also detect an absorption in the LW flux at high latitudes, that is

1835 absent at midlatitudes, where this T50 warming is evident of the potential role of a decreased

1836 temperature gradient in the polar vortex weakening identified. Furthermore, the upward wave flux

1837 from the troposphere into the stratosphere and the T50 warming indicate absorption of upward

1838 propagating waves into the stratosphere that causes this warming and weakening of U10 winds

1839 over the polar cap. This pattern is known to be related to SSWs (Kretschmer et al., 2018; Kodera

1840 et al., 2016) that we further confirm in winter 3.

1841 Although the above coincides with a positive (negative) eddy feedback in the first (second) winter

1842 that could in theory play a role in sustaining the strengthening (weakening) of the polar vortex, our

1843 eddy feedback results indicate low signal to noise where further studies with additional ensemble

1844 members would be required to confirm their role in the forced response. Similarly as the eddy

1845 feedback, low signal to noise is also evident in the SSW analysis, both of which suggest the need

1846 for more ensemble members in order to get a more robust response. However, the response we do

1847 detect in the U50 and T50 fields is strong compared to the unperturbed run where the eddy

1848 feedback, and especially the SSW, provides an explanation in agreement with the patterns detected

1849 although noisy.

1850

1851 Bittner et al. (2016b) identified a similar but opposite response, when compared to our *cpl* response

1852 in winters 2-3 (Fig. 4), following a Tambora-like eruption where a strengthening of the polar vortex

1853 due to less wave breaking at high latitudes was considered to be an indirect effect associated with

1854 a changes in planetary wave propagation. Since the volcanic aerosols in our experiments have

1855 declined extensively in the third winter, making the aerosol thermal forcing a limited factor, we

1856 cannot rule out similar indirect effects where changes in wave propagation leads to an increase in

1857 wave breaking at high latitudes and hence the increase in SSWs.

1858 While not directly comparable to our study but still providing an important analog, Muthers et al.

1859 (2016) identified an average increase in the number of SSWs during a 30-year (constant) decrease

1860 in solar radiation in line with our significant increase in SSWs in winter 3. Our results do support

1861 the findings of Sjolte et al. (2019), where the stratospheric temperature gradient does not appear

1862 to play a major role in the polar vortex weakening we identify but rather the upward wave flux.

1468 The strong surface cooling detected in Fig. 7 is a well-known caveat in the CMIP5 models
1469 (including CESM1) (Driscoll et al., 2012; Chylek et al., 2020) and is clearly detected in our
1470 coupled simulation. Since our results indicate the dominant role of the volcanically induced
1471 stratospheric thermal wind balance that causes the polar vortex strengthening, the cooling does not
1472 appear to impact the response identified in winter 1 as also revealed by the EP flux in addition to
1473 the eddy feedback although weakly. The same cannot be said about winters 2-3, where our results
1474 indicate that the exaggerated spatiotemporal T2m pattern might explain the strong upward wave
1475 flux and the associated stratospheric response.
1476 As mentioned in the methods, we assume a similar lifetime of volcanic aerosols at 65° N as at 45°
1477 N. When considering the e-folding time in Toohey et al. (2019), a substantial aerosol decrease of
1478 about 43% occurs at 17km (a.b.s.) for an eruption at 60° compared to at 0°. However, since our
1479 experiment assumes a constant stratospheric injection over 5 months with the aim to simulate a
1480 long-lasting HL eruption compared to a single injection at low latitudes, the difference in the e-
1481 folding time between low and high-latitudes would be expected to decrease. Using CESM2-
1482 WACCM6 with interactive chemistry Zhuo et al., (2023) identified that although an eruption at
1483 64° N did have a shorter aerosol lifetime compared to at 15° N, they lead to stronger volcanic
1484 forcing over the NH extratropics although the resulting climate impacts did not last as long. In
1485 addition, one of their conclusions was that different duration and intensity of both tropical and NH
1486 extratropical eruptions can lead to different results, stressing that our 6 month long sulfate injection
1487 is not directly comparable with volcanic eruptions of shorter duration. Although the aerosol
1488 lifetime in our experiment might be exaggerated into the third year, our results do indicate that the
1489 polar vortex weakening in winter 2 appears to act as a trigger for further weakening that eventually
1490 leads to SSWs in winter 3. In order to confidently confirm such a delayed link, additional
1491 sensitivity simulations are required and thus we leave that for future studies.

1492

1493 Unlike our simulated eruption using a version of WACCM4 where the chemistry is prescribed,
1494 natural volcanic eruptions can contain various chemical compounds that impact the formation and
1495 the lifetime of sulfate aerosols as well as affecting the atmospheric circulation via e.g. ozone
1496 depletion like halogens are known to do. More advanced versions as well as models that include
1497 interactive chemistry are thus important to reveal in more detail the chemistry-climate interactions
1498 that occur in the natural world (Clyne et al., 2021; Case et al., 2023; Fuglestvedt et al., 2024). Thus

Deleted: and 8

Formatted: Font colour: Auto, Ligatures: Standard + Contextual

Formatted: Font colour: Auto, Ligatures: Standard + Contextual

Deleted: Furthermore, the stratospheric aerosol warming appears to be exaggerated in *atm-only* when compared to T50 fields from the coupled simulation while the strong surface cooling is absent. In other words, *atm-only* (WACCM4) exaggerates stratospheric warming of volcanic aerosols while the coupled version exaggerates volcanic surface cooling.

Formatted: Font colour: Auto, Ligatures: Standard + Contextual

Deleted: This exaggeration could also be attributed to the volcanic forcing being zonally symmetric and thus nearly homogeneously spread throughout the higher northern latitudes during peak forcing. However, the volcanic forcing is the same in *atm-only* and coupled experiments suggesting an intrinsic reason originating in the model itself. When the idealized volcanic forcing profile is compared to the other profiles used for scaling (Fig. 1), with the aerosol lifetime being around 36 months for all curves, we would not expect drastic changes using a shorter eruption of similar injection size.¶
Although we do not focus specifically on the QBO, it is undeniably a dominating variability within the equatorial stratosphere that can influence the polar vortex differently depending on the state of the QBO. Each QBO cycle spans around 28 months on average but the number of ensemble members we have is only 20 and so we do not capture a complete QBO cycle in our *cpl* experiment. The potential impact this could have on our results was tested and from that it is clear that our *cpl* experiment is biased towards the easterly phase, where it is present in 14 ensemble members prior to the onset of our idealized volcanic eruption compared to the first 6 ensemble members having the westerly phase. The easterly phase of the QBO can impact the polar vortex by weakening it (Labe et al., 2019), thus allowing SSW events to develop more easily. To test the robustness of our results and the detected SSW in winter 3 with respect to the QBO, we also compared the

our idealized experiment can be considered primitive in the sense that it only considers sulfate aerosols but sufficient when focusing on answering questions on the basic mechanism that such eruptions can initiate. Another important aspect that we do not focus on in our study is the role of different initial conditions on the forced climate response, where initial atmospheric and climate conditions, including e.g. the stability of the polar vortex, control the lifetime and distribution of the volcanic aerosols as well as the forced dynamic climate response (Weierbach et al., 2023; Zhuo et al., 2023; Fuglestvedt et al., 2024). An exception is our assessment on how the easterly and westerly phase of the Quasi-Biennial-Oscillation affect our results where we compared ensemble members showing easterly phase with the westerly ones to test if the U50 and T50 response patterns would be different. They were not, both phases showed a weakening of the U50 although the zonal winds were more confined and consistent over the higher latitudes of the NH during the easterly phase (not shown). The difference in the number of ensemble members used for these calculations could of course impact the statistics of this test of ours but not the overall pattern detected.

CESM2-WACCM6 has obvious improvements when compared to CESM1-WACCM4 (see e.g. Gettleman et al., 2019, Danabasoglu et al., 2020), among them being an interactive QBO as well as having a slightly higher frequency of occurring SSWs (Holland et al., 2024). Nonetheless, CESM1-WACCM4 has comparable transient climate response to CESM2 as well as the ability to capture the general physical mechanism occurring within the climate system as identified in various recent studies (Danabasoglu et al., 2020; Zang et al., 2018; Elsbury et al., 2021b; Peings et al., 2023; Ding et al., 2023; Yu et al., 2024).

5 Conclusions

Results from our study suggest that two mechanisms are competing in the first three winters:

i) Winter 1: The stratospheric polar vortex strengthening is triggered by stratospheric aerosol thermal forcing via thermal wind balance. Since this response is not influenced by the strong upward wave flux identified, this is evident of two mechanisms that are competing simultaneously: A Top-down and a Bottom-up mechanism, where the Top-down dominates the response.

ii) Winter 2: The upward wave flux, originating in the strong volcanically induced surface cooling, gets absorbed in the stratosphere that causes a warming over the polar cap in addition to polar

vortex weakening. This pattern is similar to SSWs although its occurrence is not significant. Here the Bottom-up mechanism dominates.

iii) Winter 3: The persistence of the upward wave flux continuing into the third winter leads to a significant increase in SSWs with warming now confined over the polar cap, again demonstrating the dominating Bottom-up mechanism as in winter 2.

Although we do find similarities in the eddy feedback when compared to the general climate signal that we identify, such as the decrease in eddy feedback in winter 1 potentially sustaining the polar vortex strengthening, we underline its weak signal. This also applies to the SSW results although they are more clearly in support of our results.

At the same time we encourage further studies on this subject, especially concerning the lack of published comparison studies regarding both high and low latitude volcanic eruptions and SSWs. Ideally such studies would include the latest model generations in addition to observational datasets as well as consider the impact of different climate realizations and the eruption magnitude on the forced response. Furthermore, these results highlight the importance of including high-latitude volcanic forcing simulations of various lengths and/or magnitudes in projects such as VolMIP, especially considering the current volcanic unrest and increased activity in some of the major volcanic systems in Iceland.

Currently, work is ongoing to test the sensitivity of the polar vortex and the emerging SSWs to NH eruptions that are smaller in magnitude as well as the long-term climate impacts.

Data availability

The model output is available upon request by contacting the corresponding author.

Author contribution

HG conceptualized this study along with GM, YP and DZ. *Cpl* and *atm-only* experiments were carried out by HG and YP. Analysis and calculations of model output as well as graphical representation was done by HG except for the eddy feedback that was done by YP. Manuscript draft was done by HG and editing was done by DZ and YP. GM served as the principal investigator of this work and did the final editing.

28

Competing interests

The corresponding author declares that none of the authors have any competing interest.

29

References

Azoulay, A., Schmidt, H., & Timmreck, C. (2021). The Arctic polar vortex response to volcanic forcing of different strengths. *Journal of Geophysical Research: Atmospheres, 126*(11), e2020JD034450.

Baldwin, M. P., & Dunkerton, T. J. (1999). Propagation of the Arctic Oscillation from the stratosphere to the troposphere. *Journal of Geophysical Research: Atmospheres, 104*(D24), 30937-30946.

Barsotti, S., Di Rienzo, D. I., Thordarson, T., Björnsson, B. B., & Karlsdóttir, S. (2018). Assessing impact to infrastructures due to tephra fallout from Öræfajökull volcano (Iceland) by using a scenario-based approach and a numerical model. *Frontiers in Earth Science*, 6, 196.

Bittner M, Schmidt H, Timmreck C, Sienz F. Using a large ensemble of simulations to assess the Northern Hemisphere stratospheric dynamical response to tropical volcanic eruptions and its uncertainty. *Geophys Res Lett*. 2016;43(17):9324–32.

Brayshaw, D. J., B. Hoskins, and M. Blackburn, 2009: The basic ingredients of the North Atlantic storm track. Part I: Land–sea contrast and orography. *J. Atmos. Sci.*, **66**, 2539–2558, https://doi.org/10.1175/2009JAS3078.1.

Brown, F., Marshall, L., Haynes, P. H., Garcia, R. R., Birner, T., & Schmidt, A. (2023). On the magnitude and sensitivity of the quasi-biennial oscillation response to a tropical volcanic eruption. *Atmospheric Chemistry and Physics, 23*(9), 5335-5353.

Brugnatelli, V., & Tibaldi, A. (2020). Effects in North Africa of the 934–940 CE Eldgjá and 1783–1784 CE Laki eruptions (Iceland) revealed by previously unrecognized written sources. *Bulletin of Volcanology, 82*(11), 73.

Case, P., Colarco, P. R., Toon, B., Aquila, V., & Keller, C. A. (2023). Interactive stratospheric aerosol microphysics-chemistry simulations of the 1991 Pinatubo volcanic aerosols with newly

coupled sectional aerosol and stratosphere-troposphere chemistry modules in the NASA GEOS Chemistry-Climate Model (CCM). *Journal of Advances in Modeling Earth Systems*, *15*(8), e2022MS003147.

Charlton, A. J., & Polvani, L. M. (2007). A new look at stratospheric sudden warmings. Part I: Climatology and modeling benchmarks. *Journal of climate*, *20*(3), 449-469.

Church, J.A., White, N.J., Arblaster, J.M., 2005. Significant decadal-scale impact of volcanic eruptions on sea level and ocean heat content. *Nature* 438 (7064), 74–77.

Chylek, P., Folland, C., Klett, J. D., & Dubey, M. K. (2020). CMIP5 climate models overestimate cooling by volcanic aerosols. *Geophysical Research Letters*, *47*(3), e2020GL087047.

Clyne, M., Lamarque, J.-F., Mills, M. J., Khodri, M., Ball, W., Bekki, S., Dhomse, S. S., Lebas, N., Mann, G., Marshall, L., Niemeier, U., Poulain, V., Robock, A., Rozanov, E., Schmidt, A., Stenke, A., Sukhodolov, T., Timmreck, C., Toohey, M., Tummon, F., Zanchettin, D., Zhu, Y., and Toon, O. B.: Model physics and chemistry causing intermodel disagreement within the VolMIP-Tambora Interactive Stratospheric Aerosol ensemble, Atmos. Chem. Phys., 21, 3317–3343, https://doi.org/10.5194/acp-21-3317-2021, 2021.

Colose CM, LeGrande AN, Vuille M. Hemispherically asymmetric volcanic forcing of tropical hydroclimate during the last millennium. *Earth Sys Dyn*. 2016;7(3):681–96. doi:10.5194/esd-7-681-2016.

DallaSanta, K., Gerber, E. P., & Toohey, M. (2019). The circulation response to volcanic eruptions: The key roles of stratospheric warming and eddy interactions. *Journal of Climate*, *32*(4), 1101-1120.

DallaSanta, K., & Polvani, L. M. (2022). Volcanic stratospheric injections up to 160 Tg (S) yield a Eurasian winter warming indistinguishable from internal variability. *Atmospheric Chemistry and Physics*, *22*(13), 8843-8862.

31

Danabasoglu, G., Lamarque, J. F., Bacmeister, J., Bailey, D. A., DuVivier, A. K., Edwards, J., ... & Strand, W. G. (2020). The community earth system model version 2 (CESM2). *Journal of Advances in Modeling Earth Systems*, *12*(2), e2019MS001916.

Dee, S. G., Cobb, K. M., Emile-Geay, J., Ault, T. R., Edwards, R. L., Cheng, H., & Charles, C. D. (2020). No consistent ENSO response to volcanic forcing over the last millennium. *Science*, *367*(6485), 1477-1481.

Ding, X., Chen, G., Zhang, P., Domeisen, D. I., & Orbe, C. (2023). Extreme stratospheric wave activity as harbingers of cold events over North America. *Communications Earth & Environment*, *4*(1), 187.

Domeisen, D. I., Grams, C. M., & Papritz, L. (2020). The role of North Atlantic–European weather regimes in the surface impact of sudden stratospheric warming events. *Weather and Climate Dynamics*, *1*(2), 373-388.

Driscoll, S., Bozzo, A., Gray, L. J., Robock, A., Stenchikov, G., 2012. Coupled ModelIntercomparison Project 5 (CMIP5) simulations of climate following volcanic erup-tions. *J. Geophys. Res.: Atmospheres,* 117 (D17).

Edmon, H.J., Hoskins, B.J. and McIntyre, M.E. (1980) Eliassen-Palm cross sections for the troposphere. *Journal of the Atmospheric Sciences*, **37**, 2600–2616.

Einarsson, P. (2019). Historical accounts of pre-eruption seismicity of Katla, Hekla, Öræfajökull and other volcanoes in Iceland. *Jökull*, *69*, 35-52.

Elsbury, D., Y. Peings and G. Magnusdottir, 2021b. Variation in the Holton-Tan effect by longitude. Quarterly Journal of the Royal Meteorological Society. DOI: 10.1002/qj.3993

Elsbury, D., Peings, Y., & Magnusdottir, G. (2021). CMIP6 models underestimate the Holton-Tan effect. *Geophysical Research Letters*, *48*(24), e2021GL094083.

Fischer, H., Siggaard-Andersen, M.L., Ruth, U., Röthlisberger, R., Wolff, E., 2007. Glacial/interglacial changes in mineral dust and sea-salt records in polar ice cores: Sources,transport, and deposition. *Rev. Geophys*. (1), 45.

Fuglestvedt, H. F., Zhuo, Z., Toohey, M., & Krüger, K. (2024). Volcanic forcing of high-latitude Northern Hemisphere eruptions. *npj Climate and Atmospheric Science*, *7*(1), 10.

Gettelman, A., Mills, M. J., Kinnison, D. E., Garcia, R. R., Smith, A. K., Marsh, D. R., ... & Randel, W. J. (2019). The whole atmosphere community climate model version 6 (WACCM6). *Journal of Geophysical Research: Atmospheres*, *124*(23), 12380-12403.

Gettelman, A., Schmidt, A., & Egill Kristjánsson, J. (2015). Icelandic volcanic emissions and climate. *Nature Geoscience*, *8*(4), 243-243.

Gleckler, P.J., AchutaRao, K., Gregory, J.M., Santer, B.D., Taylor, K.E., Wigley, T.M.L.,2006. Krakatoa lives: The effect of volcanic eruptions on ocean heat content and thermal expansion. Geophys. Res. Lett. (17), 33.

Graf, H.F., Perlwitz, J., Kirchner, I., 1994. Northern hemisphere tropospheric midlatitude circulation after violent volcanic eruptions. Contr. Atmos. Physics 67 (1), 3–13

Graf, H.-F., D. Zanchettin, C. Timmreck and M. Bittner (2014) Observational constraints on the tropospheric and near-surface winter signature of the Northern Hemisphere stratospheric polar vortex. Clim. Dyn., 43: 3245, doi:10.1007/s00382-014-2101-0

Guðlaugsdóttir, H., Steen-Larsen, H. C., Sjolte, J., Masson-Delmotte, V., Werner, M., & Sveinbjörnsdóttir, Á. E. (2018). The influence of volcanic eruptions on weather regimes over the North Atlantic simulated by ECHAM5/MPI-OM ensemble runs from 800 to 2000 CE. *Atmospheric Research*, *213*, 211-223.

Guðlaugsdóttir, H., Sjolte, J., Sveinbjörnsdóttir, Á. E., Werner, M., & Steen-Larsen, H. C. (2019). North Atlantic weather regimes in δ18O of winter precipitation: isotopic fingerprint of the response in the atmospheric circulation after volcanic eruptions. *Tellus B: Chemical and Physical Meteorology*, *71*(1), 1633848.

Haynes, P. H. (2005). Stratospheric dynamics. *Ann. Rev. Fluid Mech.* doi: *10.1146/annurev.fluid.37.061903.175710*

He, Y., Huang, J. & Ji, M. Impact of land–sea thermal contrast on interdecadal variation in circulation and blocking. *Clim Dyn* **43**, 3267–3279 (2014). https://doi.org/10.1007/s00382-014-2103-y

Holland, M. M., Hannay, C., Fasullo, J., Jahn, A., Kay, J. E., Mills, M., ... & Bailey, D. (2024). New model ensemble reveals how forcing uncertainty and model structure alter climate simulated across CMIP generations of the Community Earth System Model. *Geoscientific Model Development*, *17*(4), 1585-1602.

Hoskins, B. J., and P. J. Valdes, 1990: On the existence of storm-tracks. *J. Atmos. Sci.*, **47**, 1854–1864, https://doi.org/10.1175/1520-0469(1990)047<1854:OTEOST>2.0.CO;2.

Huang, J., Hitchcock, P., Maycock, A. C., McKenna, C. M., & Tian, W. (2021). Northern hemisphere cold air outbreaks are more likely to be severe during weak polar vortex conditions. *Communications Earth & Environment*, *2*(1), 147.

Hurrell, J.W., 1995. Decadal trends in the north atlantic oscillation: regional tempera-tures and precipitation. Science 269 (5224), 676–679.

Hurrell, J. W., Holland, M. M., Gent, P. R., Ghan, S., Kay, J. E., Kushner, P. J., ... & Marshall, S. (2013). The community earth system model: a framework for collaborative research. *Bulletin of the American Meteorological Society*, *94*(9), 1339-1360.

Ineson, S., Dunstone, N. J., Scaife, A. A., Andrews, M. B., Lockwood, J. F., & Pang, B. (2024). Statistics of sudden stratospheric warmings using a large model ensemble. *Atmospheric Science Letters, 25*(3), e1202.

Jungclaus, J. H., Bard, E., Baroni, M., Braconnot, P., Cao, J., Chini, L. P., Egorova, T., Evans, M., González-Rouco, J. F., Goosse, H., Hurtt, G. C., Joos, F., Kaplan, J. O., Khodri, M., Klein Goldewijk, K., Krivova, N., LeGrande, A. N., Lorenz, S. J., Luterbacher, J., Man, W., Maycock, A. C., Meinshausen, M., Moberg, A., Muscheler, R., Nehrbass-Ahles, C., Otto-Bliesner, B. I., Phipps, S. J., Pongratz, J., Rozanov, E., Schmidt, G. A., Schmidt, H., Schmutz, W., Schurer, A., Shapiro, A. I., Sigl, M., Smerdon, J. E., Solanki, S. K., Timmreck, C., Toohey, M., Usoskin, I. G., Wagner, S., Wu, C.-J., Yeo, K. L., Zanchettin, D., Zhang, Q., and Zorita, E.: The PMIP4 contribution to CMIP6 – Part 3: The last millennium, scientific objective, and experimental design for the PMIP4 past1000 simulations, Geosci. Model Dev., 10, 4005-4033, https://doi.org/10.5194/gmd-10-4005-2017, 2017

Khodri, M., Izumo, T., Vialard, J., Janicot, S., Cassou, C., Lengaigne, M., et al. (2017). Tropical explosive volcanic eruptions can trigger El Niño by cooling tropical Africa. Nature Communications, 8(1), 778. https://doi.org/10.1038/s41467-017-00755-6

Kim, B.M., Son, S.W., Min, S.K., Jeong, J.H., Kim, S.J., Zhang, X., Shim, T., Yoon, J.H.,2014. Weakening of the stratospheric polar vortex by arctic sea-ice loss. Nat.Commun. 5, 4646.

Kodera, K., 1994. Influence of volcanic eruptions on the troposphere through strato-spheric dynamical processes in the northern hemisphere winter. J. Geophys. Res.-Atmos. 99 (D1), 1273–1282

Kodera, K., Mukougawa, H., Maury, P., Ueda, M., & Claud, C. (2016). Absorbing and reflecting sudden stratospheric warming events and their relationship with tropospheric circulation. *Journal of Geophysical Research: Atmospheres, 121*(1), 80-94.

Kolstad, E. W., Lee, S. H., Butler, A. H., Domeisen, D. I., & Wulff, C. O. (2022). Diverse surface signatures of stratospheric polar vortex anomalies. *Journal of Geophysical Research: Atmospheres, 127*(20), e2022JD037422.

Kretschmer, M., Cohen, J., Matthias, V., Runge, J., & Coumou, D. (2018). The different stratospheric influence on cold-extremes in Eurasia and North America. *npj Climate and Atmospheric Science, 1*(1), 44.

Labe, Z., Peings, Y., & Magnusdottir, G. (2019). The effect of QBO phase on the atmospheric response to projected Arctic sea ice loss in early winter. *Geophysical Research Letters, 46*(13), 7663-7671.

Larsen, G., & Gudmundsson, M. T. (2014). Volcanic system: Bárðarbunga system. *Catalogue of Icelandic Volcanoes*, 1-11.

Lehtonen, I., & Karpechko, A. Y. (2016). Observed and modeled tropospheric cold anomalies associated with sudden stratospheric warmings. *Journal of Geophysical Research: Atmospheres, 121*(4), 1591-1610.

Meronen, H., Henriksson, S. V., Räisänen, P., & Laaksonen, A. (2012). Climate effects of northern hemisphere volcanic eruptions in an Earth System Model. *Atmospheric research, 114*, 107-118.

Muthers, S., Raible, C. C., Rozanov, E., & Stocker, T. F. (2016). Response of the AMOC to reduced solar radiation–the modulating role of atmospheric chemistry. *Earth System Dynamics, 7*(4), 877-892.

Nakamura, N. (2024). Large-Scale Eddy-Mean Flow Interaction in the Earth's Extratropical Atmosphere. *Annual Review of Fluid Mechanics, 56*(1), 349-377.

Neely III, R. R., Conley, A. J., Vitt, F., & Lamarque, J. F. (2016). A consistent prescription of stratospheric aerosol for both radiation and chemistry in the Community Earth System Model (CESM1). *Geoscientific Model Development, 9*(7), 2459-2470.

Oman, L., Robock, A., Stenchikov, G., Schmidt, G. A., & Ruedy, R. (2005). Climatic response to high-latitude volcanic eruptions. *Journal of Geophysical Research: Atmospheres, 110*(D13).

Omrani, N.-E., Keenlyside, N., Matthes, K., Boljka, L., Zanchettin, D., Jungclaus, J. H., Lubis, S. W. (2022) Coupled stratosphere-troposphere-Atlantic multidecadal oscillation and its importance for near-future climate projection. npj Climate and Atmospheric Science, 5, 59, https://doi.org/10.1038/s41612-022-00275-1

Oppenheimer, C., Orchard, A., Stoffel, M., Newfield, T. P., Guillet, S., Corona, C., ... & Büntgen, U. (2018). The Eldgjá eruption: timing, long-range impacts and influence on the Christianisation of Iceland. *Climatic Change, 147*, 369-381.Otterå, O.H., Bentsen, M., Drange, H., Suo, L., 2010. External forcing as a metronome foratlantic multidecadal variability. Nat. Geosci. 3 (10), 688–694

Ortega, P., Swingedouw, D., Masson-Delmotte, V., Risi, C., Vinther, B., Yiou, P., Vautard,R., Yoshimura, K., 2014. Characterizing atmospheric circulation signals in. Greenlandice cores: insights from a weather regime approach. Clim. Dyn. 43 (9–10),2585–2605

Otterå, O. H., Bentsen, M., Drange, H., & Suo, L. (2010). External forcing as a metronome for Atlantic multidecadal variability. *Nature Geoscience, 3*(10), 688-694.

Pausata, F. S. R., Chafik, L., Caballero, R. & Battisti, D. S. Impacts of high- latitude volcanic eruptions on ENSO and AMOC. Proc. Natl Acad. Sci. 112, 13784–13788 (2015).

Pausata, F.S.R., D. Zanchettin, C. Karamperidou, R. Caballero, and D. S. Battisti (2020) ITCZ shift and extratropical teleconnections drive ENSO response to volcanic eruptions. Science Advances 6(23) eaaz5006, doi: 10.1126/sciadv.aaz5006

Pausata, F. S. R., Zhao, Y., Zanchettin, D., Caballero, R., & Battisti, D. S. (2023). Revisiting the mechanisms of ENSO response to tropical volcanic eruptions. Geophysical Research Letters, 50, e2022GL102183. https://doi.org/10.1029/2022GL102183

Perlwitz, J., Graf, H.F., 1995. The statistical connection between tropospheric and. stra-tospheric circulation of the Northern Hemisphere in winter. J. Clim. (10),2281–2295

Peings, Y., & Magnusdottir, G. (2014). Response of the wintertime Northern Hemisphere atmospheric circulation to current and projected Arctic sea ice decline: A numerical study with CAM5. *Journal of Climate*, *27*(1), 244-264.

Peings, Y., Davini, P., & Magnusdottir, G. (2023). Impact of Ural blocking on early winter climate variability under different Barents-Kara sea ice conditions. *Journal of Geophysical Research: Atmospheres*, *128*(6), e2022JD036994.

Plumb, R. A. (1985). On the three-dimensional propagation of stationary waves. *Journal of Atmospheric Sciences*, *42*(3), 217-229.

Polvani, L. M., Banerjee, A., & Schmidt, A. (2019). Northern Hemisphere continental winter warming following the 1991 Mt. Pinatubo eruption: reconciling models and observations. *Atmospheric Chemistry and Physics*, *19*(9), 6351-6366.

Portal, A., Pasquero, C., D'andrea, F., Davini, P., Hamouda, M. E., & Rivière, G. (2022). Influence of reduced winter land–sea contrast on the midlatitude atmospheric circulation. *Journal of Climate*, *35*(19), 6237-6251.

Predybaylo, E., Stenchikov, G., Wittenberg, A. T. & Osipov, S. El Niño/ Southern Oscillation response to low-latitude volcanic eruptions depends on ocean pre-conditions and eruption timing. Commun. Earth Environ. 1, 1–13 (2020).

Rayner, N. A. A., Parker, D. E., Horton, E. B., Folland, C. K., Alexander, L. V., Rowell, D. P., ... & Kaplan, A. (2003). Global analyses of sea surface temperature, sea ice, and night marine air temperature since the late nineteenth century. *Journal of Geophysical Research: Atmospheres*, *108*(D14).

Robock, A., Mao, J., 1992. Winter warming from large volcanic eruptions. Geophys. Res.Lett. 19 (24), 2405–2408.

Robock, A., 2000. Volcanic eruptions and climate. Rev. Geophys. 38 (2), 191–219.

Screen, J. A., Deser, C., Smith, D. M., Zhang, X., Blackport, R., Kushner, P. J., ... & Sun, L. (2018). Consistency and discrepancy in the atmospheric response to Arctic sea-ice loss across climate models. *Nature Geoscience, 11*(3), 155-163.

Shindell, D.T., Schmidt, G.A., Mann, M.E., Faluvegi, G., 2009. Dynamic winter. Climate response to large tropical volcanic eruptions since 1600. J. Geophys. Res.-Atmos.(D5), 109.Sigl, M., Winstrup, M., McConnell, J.R., Welten, K.C., Plunkett, G., Ludlow, F., Buntgen,U., Caffee, M., Chellman, N., Dahl-Jensen, D., Fischer, H., 2009. Timing and climate forcing of volcanic eruptions for the past 2500 years. Nature 523 (7562), 543–549

Sjolte, J., Adolphi, F., Guðlaugsdòttir, H., & Muscheler, R. (2021). Major Differences in Regional Climate Impact Between High-and Low-Latitude Volcanic Eruptions. *Geophysical Research Letters, 48*(8), e2020GL092017.

Smith, D. M., Eade, R., Andrews, M. B., Ayres, H., Clark, A., Chripko, S., ... & Walsh, A. (2022). Robust but weak winter atmospheric circulation response to future Arctic sea ice loss. *Nature communications, 13*(1), 727.

Smith, K. L., Neely, R. R., Marsh, D. R., & Polvani, L. M. (2014). The specified chemistry whole atmosphere community climate model (SC-WACCM). *Journal of Advances in Modeling Earth Systems, 6*(3), 883-901.

Stenchikov, G., Robock, A., Ramaswamy, V., Schwarzkopf, M.D., Hamilton, K.,Ramachandran, S., 2002. Arctic Oscillation response to the 1991 Mount Pinatubo.eruption: Effects of volcanic aerosols and ozone depletion. J. Geophys. Res.-Atmos.(D24), 107.

Stenchikov, G., Delworth, T.L., Ramaswamy, V., Stouffer, R.J., Wittenberg, A., Zeng, F.,2009. Volcanic signals in oceans. J. Geophys. Res.-Atmos. (D16), 114.

Stothers, R. B. (1998). Far reach of the tenth century Eldgjá eruption, Iceland. *Climatic Change, 39*(4), 715-726.

Swingedouw, D., Ortega, P., Mignot, J., Guilyardi, E., Masson-Delmotte, V., Butler, P.G.,Khodri, M., Séférian, R., 2015. Bidecadal North Atlantic ocean circulation variability controlled by timing of volcanic eruptions. Nat. Commun. 6, 6545.

Thomas, M. A., Giorgetta, M. A., Timmreck, C., Graf, H. F., & Stenchikov, G. (2009). Simulation of the climate impact of Mt. Pinatubo eruption using ECHAM5–Part 2: Sensitivity to the phase of the QBO and ENSO. *Atmospheric Chemistry and Physics, 9*(9), 3001-3009.

Timmreck, C.: Modeling the climatic effects of large explosive volcanic eruptions, Wiley Interdisciplinary Reviews: Climate Change, 3, 545–564, 2012.

Thordarson, T., & Self, S. (2003). Atmospheric and environmental effects of the 1783–1784 Laki eruption: A review and reassessment. *Journal of Geophysical Research: Atmospheres, 108*(D1), AAC-7.

Thordarson, T., Miller, D. J., Larsen, G., Self, S., & Sigurdsson, H. (2001). New estimates of sulfur degassing and atmospheric mass-loading by the 934 AD Eldgjá eruption, Iceland. *Journal of Volcanology and Geothermal Research, 108*(1-4), 33-54.

Toohey, M., Stevens, B., Schmidt, H., & Timmreck, C. (2016). Easy Volcanic Aerosol (EVA v1. 0): an idealized forcing generator for climate simulations. *Geoscientific Model Development, 9*(11), 4049-4070.

Toohey, M., Krüger, K., Schmidt, H., Timmreck, C., Sigl, M., Stoffel, M., & Wilson, R. (2019). Disproportionately strong climate forcing from extratropical explosive volcanic eruptions. Nature Geoscience, 12(2), 100-107.

Toohey, M., Krüger, K., Bittner, M., Timmreck, C., and Schmidt, H.: The impact of volcanic aerosol on the Northern Hemisphere stratospheric polar vortex: mechanisms and sensitivity to forcing structure, Atmos. Chem. Phys., 14, 13063–13079, https://doi.org/10.5194/acp-14-13063-2014, 2014.

Wake, B. Land–sea contrast. *Nature Clim Change* 4, 326 (2014). https://doi.org/10.1038/nclimate2233

Weierbach, H., LeGrande, A. N., and Tsigaridis, K.: The impact of ENSO and NAO initial conditions and anomalies on the modeled response to Pinatubo-sized volcanic forcing, Atmos. Chem. Phys., 23, 15491–15505, https://doi.org/10.5194/acp-23-15491-2023, 2023.

Yu, Q., Wu, B., & Zhang, W. (2024). The atmospheric connection between the Arctic and Eurasia is underestimated in simulations with prescribed sea ice. *Communications Earth & Environment*, *5*(1), 435.

Zambri, B., Robock, A., Mills, M. J., & Schmidt, A. (2019). Modeling the 1783–1784 Laki eruption in Iceland: 2. Climate impacts. *Journal of Geophysical Research: Atmospheres, 124*(13), 6770-6790.

Zanchettin, D., Timmreck, C., Graf, H.F., Rubino, A., Lorenz, S., Lohmann, K., Jungclaus,J.H., 2012. Bi-decadal variability excited in the coupled ocean-atmosphere system by strong tropical volcanic eruptions. Clim. Dyn. 39 (1–2), 419–444.

Zanchettin, D., Timmreck, C., Bothe, O., Lorenz, S.J., Hegerl, G., Graf, H.F., Lutherbacher,J., Jungclaus, J.H., 2013. Delayed winter warming: A robust decadal response to strong tropical volcanic eruptions. Geophys. Res. Lett. 40 (1), 204–209.

Zanchettin, D., Khodri, M., Timmreck, C., Toohey, M., Schmidt, A., Gerber, E. P., Hegerl, G., Robock, A., Pausata, F. S. R., Ball, W. T., Bauer, S. E., Bekki, S., Dhomse, S. S., LeGrande, A. N., Mann, G. W., Marshall, L., Mills, M., Marchand, M., Niemeier, U., Poulain, V., Rozanov, E., Rubino, A., Stenke, A., Tsigaridis, K., and Tummon, F.: The Model Intercomparison Project on the

climatic response to Volcanic forcing (VolMIP): experimental design and forcing input data for CMIP6, Geosci. Model Dev., 9, 2701-2719, doi:10.5194/gmd-9-2701-2016, 2016.

Zanchettin, D. (2017) Aerosol and Solar Irradiance Effects on Decadal Climate Variability and Predictability. Current Climate Change Reports, 3, 150, doi:10.1007/s40641-017-0065-y

Zanchettin, D., Timmreck, C., Khodri, M., Schmidt, A., Toohey, M., Abe, M., Bekki, S., Cole, J., Fang, S.-W., Feng, W., Hegerl, G., Johnson, B., Lebas, N., LeGrande, A. N., Mann, G. W., Marshall, L., Rieger, L., Robock, A., Rubinetti, S., Tsigaridis, K., and Weierbach, H.: Effects of forcing differences and initial conditions on inter-model agreement in the VolMIP volc-pinatubo-full experiment, Geosci. Model Dev., 15, 2265–2292, https://doi.org/10.5194/gmd-15-2265-2022, 2022

Zhang P, Wu Y, Simpson IR, Smith KL, Zhang X, De B, Callaghan P. A stratospheric pathway linking a colder Siberia to Barents-Kara Sea sea ice loss. Sci Adv. 2018 Jul 25;4(7):eaat6025. doi: 10.1126/sciadv.aat6025. PMID: 30050990; PMCID: PMC6059732.

Zhu, F., Emile-Geay, J., Anchukaitis, K. J., Hakim, G. J., Wittenberg, A. T., Morales, M. S., ... & King, J. (2022). A re-appraisal of the ENSO response to volcanism with paleoclimate data assimilation. *Nature communications, 13*(1), 747.

Zhuo, Z., Fuglestvedt, H. F., Toohey, M., & Krüger, K. (2023). Initial conditions control transport of volcanic volatiles, forcing and impacts. *EGUsphere, 2023*, 1-26.